Available online at www.sciencedirect.com
ScienceDirect
Journal of Catalysis 243 (2006) 199–211
JOURNAL OF CATALYSIS
www.elsevier.com/locate/jcat

Genesis of iron carbides and their role in the synthesis of hydrocarbons from synthesis gas

Tirma Herranz, Sergio Rojas *, Francisco J. Pérez-Alonso, Manuel Ojeda, Pilar Terreros, José Luis G. Fierro *

Instituto de Catálisis y Petroleoquímica (CSIC), C/Marie Curie 2, 28049 Madrid, Spain

Received 24 April 2006; revised 22 June 2006; accepted 11 July 2006

Abstract

A series of iron-based Fischer–Tropsch catalysts, either pure or promoted with Ce or Mn, were subjected to different activation treatments with H_2, CO, or H_2/CO. The surface species formed after different treatments were characterized by temperature-programmed surface reaction with hydrogen (TPSR-H_2) and temperature-programmed surface desorption with argon (TPD-Ar). After activation and temperature-programmed treatments, the samples were passivated and characterized by X-ray diffraction and Raman spectroscopy. After each activation treatment, the catalysts were tested in the Fischer–Tropsch synthesis, and selected postreaction samples were characterized by Mössbauer spectroscopy. After CO and syngas treatment, cementite (θ-Fe_3C) and Hägg (χ-$Fe_{2.5}C$) carbides were formed, respectively. Different surface carbonaceous species were stabilized over these carbides. Cementite species are less active in the Fischer–Tropsch synthesis; however, under the Fischer–Tropsch reaction environment, they can evolve into the Hägg carbide, over which the more active carbonaceous intermediate species are formed. Modification of the catalyst composition by Mn and Ce is effective only when the samples are activated under CO, accelerating the stabilization of active carbonaceous intermediates.

Keywords: Activation treatment; Fischer–Tropsch; TPD (TPSR); CO; Iron carbides; Manganese oxide; Cerium oxide

1. Introduction

Hydrocarbon production via Fischer–Tropsch synthesis (FTS) is receiving a renewed interest for both industrial and academic applications. FTS renders sulfur- and aromatic-free liquid fuels along with valuable intermediates (mainly alcohols and alkenes) from syngas. The major drawback hindering wider implementation of FTS relates to its financial competitiveness. However, issues associated to the current oil extraction and transformation technologies, such as more stringent environmental regulations, the tremendous rise of oil prices and the need for further investments within the refinery sector, are making FTS (or, in a wider sense, the gas-to-liquids process) more attractive and feasible for hydrocarbon production.

The oxides of groups 8, 9, and 10 metals (Co, Ni, Ru, and Fe) are the archetypal catalysts precursors used in FTS. Because the oxide form is inactive for the reaction, the solids must be subjected to an activation treatment to obtain the actual Fischer–Tropsch catalyst. Cobalt-, nickel-, and ruthenium-based solids require an H_2 treatment at temperatures between 473 and 723 K to become active, remaining in their metallic state during FTS [1]. However, the activation process is not so simple for the iron-based catalysts that have been reported to be activated under carbon monoxide [2,3], hydrogen [4], or synthesis gas [5–8] treatments.

During the pretreatment step and even during FTS, Fe-based catalysts may develop several phase transformations. The nature of the final phase(s) after the pretreatment, or, more likely, the more stable phase(s) under FTS, will determine the performance of the catalyst. During the activation process, iron oxide first transforms from hematite (α-Fe_2O_3) to magnetite (Fe_3O_4) irrespective of the activation gas used for pretreatment. From

* Corresponding authors.
E-mail addresses: srojas@icp.csic.es (S. Rojas), jlgf@icp.csic.es (J.L.G. Fierro).

0021-9517/$ – see front matter
doi:10.1016/j.jcat.2006.07.012

this point, the nature of the activating atmosphere will determine the nature of the Fe phases formed. Under CO or syngas pretreatment, iron carbide phases are formed. Among these, O carbides (carbides with carbon atoms in octahedral interstices, ε-Fe_2C, ε'-$Fe_{2.2}C$, and Fe_xC) and TP carbides (carbides with carbon atoms in trigonal prismatic interstices, χ-$Fe_{2.5}C$ and θ-Fe_3C) have been identified [9]. Hydrogen activation of iron-based samples yields metallic iron (Fe^0), which evolves into iron carbide species under the FTS environment (syngas) [10]. Furthermore, the actual nature of the Fe phases formed during the different pretreatments depends on the time of exposure to the reactant feed, the composition of the feed, the reactor system, and the activation conditions (temperature and pressure) [11].

Despite the controversy concerning the actual nature of the active phases [12–14], a correlation between the carbide content and the Fischer–Tropsch activity has been widely observed [2,11,15,16]. Two models have been proposed to explain the role of the carbide phase. On the one hand, the carbide model [17] proposes that FTS occurs in the surface of a bulk iron carbide phase; being the density of such sites dependent on the extent of the bulk carburization. On the other hand, the competition model [18] proposes that one or more carbon atoms together with metallic iron form the active site at which the carbon atoms are hydrogenated. Iron carburization and hydrocarbon formation from surface "C-containing" species occur simultaneously in a competitive reaction. It should be noted that on either model, Fe carbide formation is a necessary step to yield the actual FTS catalyst. However, the correlation between bulk carbide species, surface carbon species, and catalytic activity has not yet been established. Neither has the actual role of the carbide species in FTS been established; whether they are really involved in the reaction or they are mere spectators is a matter of debate. Moreover, a lack of correlation between the amount of bulk iron carbide and the activity of the Fe catalyst has been reported [4,19].

Recently, Bartholomew et al. [20,21] identified and quantified several carbon and metal carbide species on the surface of unsupported and supported used Fe catalysts by means of temperature-programmed surface reaction with hydrogen (TPSR-H_2). In both systems, good correlation between the coverage of atomic surface carbon species and their catalytic performance was found. However, pinpointing the nature of the species formed after the activation treatment, correlating their presence and abundance with the different activation treatments and identifying the optimum activation treatment remain subjects for future study.

Consequently, the present work was undertaken to provide a detailed characterization study of iron-based FTS catalysts subjected to CO (pure and diluted), hydrogen, or syngas (H_2/CO) pretreatment to determine the most effective activation method, as well as the nature of the bulk and surface species formed during the different pretreatments. The study was conducted over pure iron oxide and Mn- and Ce-modified iron samples. The characterization results were correlated with the catalytic activity measurements. Manganese is known to be an important promoter for improving the yield to light olefins [22], and cerium recently has been reported as a good structural promoter [23]. This approach has provided valuable information about the influence of the activation treatment as a function of the catalyst nature. For the oxide-modified samples, the influence of Mn and Ce on the activation process has also been characterized. To date, the role of K and C as additives in the activation treatment has been rarely studied [24,25], and only a few works have dealt with the role of Mn [26,27]. To the best of our knowledge, the effect of adding Ce to Fe-based catalysts on the activation process has not yet been reported.

The catalysts were characterized in situ after each activation method by surface techniques, including TPSR-H_2 and temperature-programmed surface desorption with argon (TPD-Ar). The samples were then further characterized (after careful passivation) by X-ray diffraction, Raman spectroscopy, and Mössbauer spectroscopy to obtain information about their bulk composition after activation and reaction.

2. Experimental

The experimental procedure for sample preparation has been described previously [23,28]. Briefly, sample 100Fe was prepared by precipitation of a solution of $Fe(NO_3)_3{\cdot}9H_2O$ (Fluka, 98–100%) with an ammonia solution. The solid was dried in air at 343 K and calcined at 573 K for 6 h. Sample 95Fe5Mn, with a Fe/Mn atomic ratio of 95/5, was prepared by the microemulsion technique [29] using a water solution of $Fe(NO_3)_3{\cdot}9H_2O$ and $Mn(NO_3)_3{\cdot}4H_2O$ (Fluka, 97%) as a metal precursor. Isooctane (Aldrich, >99%) and Tergitol 15-S-5 were used as the organic phase and surfactant, respectively. An NH_4OH (Panreac, 28.0–30.0%) water in oil microemulsion was used as the precipitating agent. The solid was recovered and washed thoroughly with distilled water and ethanol several times, dried at 383 K, and calcined at 773 K for 6 h. Sample 95Fe5Ce (with a Fe/Ce atomic ratio of 95/5) was prepared by the coprecipitation method. Two water solutions of $Fe(NO_3)_3{\cdot}9H_2O$ and $Ce(NO_3)_3{\cdot}6H_2O$ (Aldrich, 99.99%) were added simultaneously to a precipitating batch containing 500 ml of distilled water. Addition of precipitating agent (NH_4OH) was accomplished using a pH-stationary device, maintaining the pH constant (at 8.0) during precipitation. The solid was recovered, washed thoroughly with distilled water at 343 K, dried in air at 353 K, and then calcined at 573 K for 6 h. Sample 70Fe30Mn (atomic ratio 70/30) was prepared by precipitating an aqueous solution of the nitrate precursors by adding an aqueous solution of NaOH. The precipitated solid was washed with water, dried in air at 353 K, and calcined in air at 773 K for 6 h.

For the temperature-programmed experiments, ca. 40 mg of the sample was loaded into a U-shaped quartz reactor. The samples were pretreated in H_2, CO, CO/Ar (5% CO), or H_2/CO (ratio 2:1) mixtures at 723 K (at a heating rate of 10 K min^{-1}) for 1 h and then flushed with Ar at 723 K for 15 min. Then the samples were cooled to room temperature under Ar flow. The reactivity of the species remaining on the surface of the solids was tested by passing Ar (TPD-Ar), H_2/Ar (10%) (TPSR-H_2), or (H_2 + CO)/Ar (10%) (TPSR-H_2-CO). The gas flow rate was 50–100 ml min^{-1}, and the temperature was increased from 298

to 1123 K at a rate of 10 K min^{-1}. The evolution of different compounds was monitored by selected m/z fragments followed by a quadrupolar mass spectrometer connected on-line to the reactor. Downstream lines were heated to 393 K to prevent condensation of products.

After the activation and the temperature-programmed treatments, the samples were passivated with an 1 vol% O_2/He mixture at room temperature for 1 h, according to a standard procedure described elsewhere [30]. Then the samples were analyzed by X-ray diffraction (XRD). Powder XRD patterns were recorded in the 10°–80° 2θ range in the scan mode (0.05°, 2 s) using a Seifert 3000 XRD diffractometer equipped with a PW goniometer with Bragg–Brentano $\theta/2\theta$ geometry, an automatic slit, and a bent graphite monochromator.

Raman spectra of passivated samples were recorded in He flow to prevent oxidation of the sample due to the heating power of the laser beam [28]. Raman spectra were collected using a single monochromator Renishaw system 1000 equipped with a thermoelectrically cooled CCD detector and holographic super-notch filter. Typically, 20 mg of a powdered sample was mounted on a treatment chamber, and the sample was excited with the 514.5-nm Ar line. The spectral resolution was ca. 3 cm^{-1}, and the spectrum acquisition time was 300 s.

The samples were tested in the CO hydrogenation reaction using a fixed-bed microreactor (stainless steel 316, 165 mm long, 8.5 mm i.d.). The reactor temperature was measured with a K-type thermocouple buried in the catalytic bed. The reactor was held within a furnace equipped with a temperature controller. All pipes after reactor outlet were kept at 433 K. The reaction system was equipped with a downstream stainless steel trap set at 353 K to collect the heavier products (C_{17+} hydrocarbons). Flow rates were controlled using Bronkhorst High-Tech Series mass flow controllers. The calcined samples (110 mg, 0.25–0.30 mm particle size) were diluted with SiC (ca. 2.5 g, 0.25–0.30 mm particle size) to avoid hot spots. First, the catalysts were activated in situ with different treatments (CO, pure or diluted with Ar, H_2/CO, or H_2) at 723 K and atmospheric pressure. The reactor was then cooled down in inert gas to the reaction temperature (573 K) and pressurized at 1.01 MPa. CO hydrogenation was measured for 10,000 min (GHSV = 0.0023 L g^{-1} s^{-1}). Analysis of reactant gases and products was performed on-line with a gas chromatograph (Varian CP-3800). A polymeric column connected to a thermal conductivity detector was used to analyze inorganic gases (H_2, N_2, CO, and CO_2) and water. Hydrocarbons and oxygenated compounds were analyzed with a Restek Rtx-1 capillary column (105 m × 0.25 mm × 0.25 μm) connected to a flame ionization detector. The following temperature program was used: 213 K for 6 min, then a ramp of 8 K min^{-1} to 498 K, maintained at this temperature for 26 min. N_2 was used as internal standard for chromatographic analyses.

After the catalytic measurements, selected samples were passivated and characterized by ^{57}Fe Mössbauer spectroscopy. Transmission Mössbauer spectra were recorded at room temperature using a conventional constant-acceleration spectrometer equipped with a ^{57}Co (Rh) source. Finely ground powdered absorbers were prepared with a natural Fe thickness of about 10 mg cm^{-2}. The spectra were computer-fitted to a sum of Lorentzian-shaped lines by applying the constraints of equal line width and area for the two peaks of doublets and equal line width and areas at a ratio of 3:2:1:1:2:3 for the six peaks of sextets. The relative concentrations of the different Fe species were calculated from their spectral area ratios assuming equal f factors (probability of Mössbauer effect) for all of the Fe species present in the spectrum. Isomer shifts were referred to the center of the α-Fe sextet at room temperature.

Scheme 1 summarizes all of the activation pretreatments and characterization techniques used in this work.

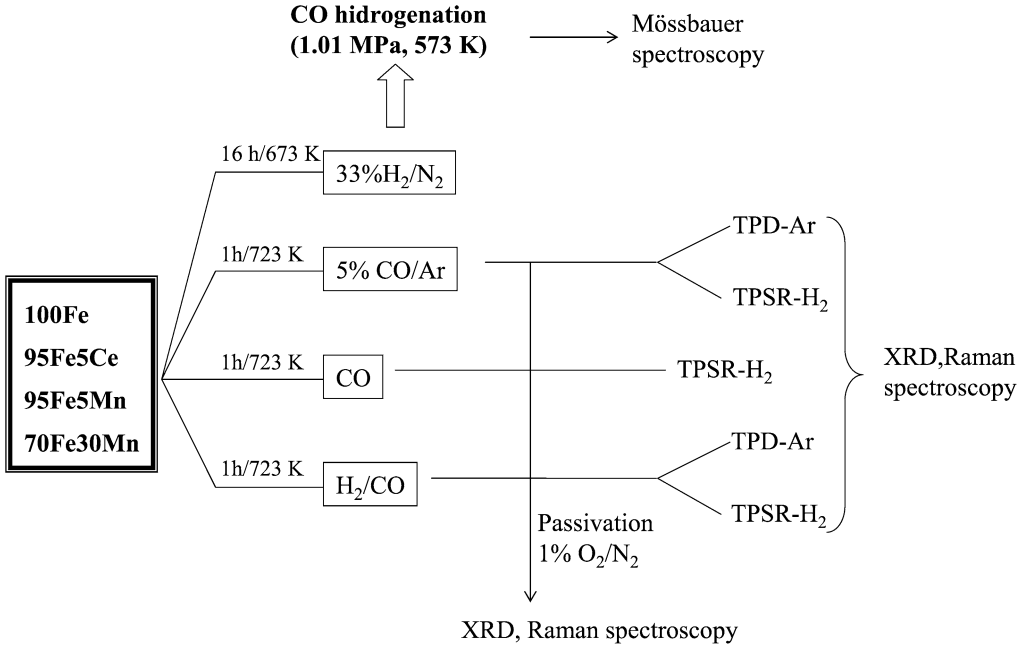

Scheme 1. Activation pretreatments and characterization techniques used.

3. Results

3.1. Catalyst characterization

We start by comparing the TPSR-H_2 results obtained with the samples pretreated in H_2/CO, CO/Ar, and CO streams. Once the samples were pretreated, the weakly adsorbed species were removed from their surface by passing an Ar flow at 723 K for 15 min. Subsequently, a TPSR-H_2 experiment was recorded. When the samples were pretreated in hydrogen, metallic iron was the only species formed (except in sample 70Fe30Mn, which also contained manganowustite), as demonstrated by the XRD analysis of the passivated samples. Therefore, the TPSR-H_2 experiments were not performed over these samples.

The TPSR-H_2 profiles of the species either desorbed (CO) or formed under the TPSR reactive atmosphere (H_2O and CH_4) depended on the nature of both the sample and the pretreatment. Water is formed from the reduction of the iron oxide, whereas CH_4 is formed from the hydrogenation of either Fe carbides and/or surface carbonaceous species, as we discuss below. Note that hydrocarbons other than methane are not formed under the TPSR-H_2 experimental conditions, regardless of the nature of the carbon source [20,21].

Fig. 1A depicts the TPSR-H_2 profiles of samples 100Fe, 95Fe5Mn, 95Fe5Ce, and 70Fe30Mn. Methane formation was observed in all cases, with the shape and the position of the peaks strongly influenced by the nature of the solids and the pretreatment step. When pretreated under syngas, the sample 100Fe formed methane in a broad peak between 900 and 1100 K. When pretreated under pure CO, methane formation on sample 100Fe occurred in three steps centered at ca. 770, 900, and 1050 K. Noticeably, when the sample was pretreated in diluted CO (5 vol% CO/Ar), water formation, centered at ca. 680 K, was observed. Immediately afterward, methane formation, showing two peaks centered at ca. 770 and 900 K, was detected. The ratio of the peak areas was reversed with respect to the methane formation peaks recorded after the CO treatment. The peak at 1050 K was not observed. For the Ce- and Mn-loaded samples, the TPSR-H_2 profiles recorded under the same conditions displayed both common and distinct features with respect to sample 100Fe. As in sample 100Fe, methane formation in the promoted samples was observed. The process was shifted to lower temperatures when the samples were pretreated under pure CO. The shape and position of the methane formation peaks were dependent on the nature of the sample and on the pretreatment. However, unlike in 100Fe, CO desorption was also detected.

As described for sample 100Fe, methane formation was preceded by a water formation process when the pretreatment was performed in 5 vol% CO/Ar flow. Because water formation was not observed after pure CO pretreatment, it is reasonable to think that water was formed as a result of reduction of the iron oxide phase. For the 5 vol% CO/Ar pretreatment, the reduction of hematite (either promoted or not) was not complete, whereas the pure CO pretreatment led to the complete reduction of the iron oxide. Therefore, in the former case, water was formed as a consequence of reduction of the iron oxide with hydrogen during the TPSR-H_2 experiment. It is noteworthy that methane formation occurs only after water is released; therefore, oxide reduction precedes carbon hydrogenation under H_2 atmosphere, that is, before the catalyst is able to form hydrocarbons. To confirm whether this behavior can be extrapolated to the actual Fischer–Tropsch atmosphere, sample 100Fe was pretreated with a 5% CO/Ar mixture, after which a temperature-programmed surface reaction with syngas ($H_2 + CO$) was recorded (Fig. 1B). It can be seen that both carbon dioxide and water (both according to reduction of the iron oxide phase) were formed before methane. Actually, CO_2 formation preceded H_2O formation, indicating that carbon monoxide was more effective than hydrogen in reducing iron oxides. However, methane formation started even when iron oxide reduction was not complete. These results suggest that hydrocarbons can be formed in the presence of Fe_3O_4 as long as sufficient reduced iron sites (most likely carburized) are available.

Noticeably, the area under the methane formation peak was smaller when the samples were pretreated with syngas (H_2/CO), as shown in Fig. 1A. This is probably due to partial formation and desorption of methane during the pretreatment step (723 K in syngas). We tested this hypothesis by performing temperature-programmed reduction experiments under syngas (TPR_{syngas}) with the different samples. The results obtained with sample 100Fe, given in Fig. 2, show that methane formation started at temperatures above 640 K.

Methane formation was not observed when the TPD experiments of pretreated samples were carried out under Ar (TPD-Ar) instead of H_2 (TPSR-H_2). In that case, CO and H_2 were the only products detected. Fig. 3 depicts the TPD-Ar profiles recorded for samples 100Fe, 95Fe5Mn, 95Fe5Ce, and 70Fe30Mn. Sample 100Fe desorbed hydrogen only in a broad peak between 950 and 1075 K. A single hydrogen peak, smaller and shifted to higher temperatures, was also observed with samples 95Fe5Mn, 95Fe5Ce, and 70Fe30Mn. For the Ce- and Mn-loaded samples, the TPD-Ar profiles also showed a CO desorption band between 700 and 1100 K. The number, position, and area of the peaks were strongly influenced by the nature of the catalyst. Thus, CO desorption for 95Fe5Mn occurred in two steps centered at 850 and 1050 K, with the last peak showing the largest area. Sample 95Fe5Ce evolved three CO desorption peaks at 750, 850, and 1050 K. The peak at 850 K displayed the largest area. In contrast, sample 70Fe30Mn showed a single broad peak between 750 and 1100 K.

In an attempt to characterize the catalysts in detail after the different pretreatments, the samples were passivated following standard procedures [30] and studied by Raman spectroscopy and XRD as depicted in Scheme 1. The results were compared with those obtained from the calcined samples.

Raman spectra of selected samples and pretreatments are depicted in Fig. 4. The spectra of the calcined samples displayed mainly the peaks described for the α-Fe_2O_3 phase [31]. In addition, samples 70Fe30Mn and 95Fe5Ce presented a band centered at ca. 650 cm^{-1} ascribed to the formation of mixed phases (Fe–Ce or Fe–Mn) [23,28]. For samples 70Fe30Mn and 95Fe5Mn, pretreatment with CO/Ar led to the formation of

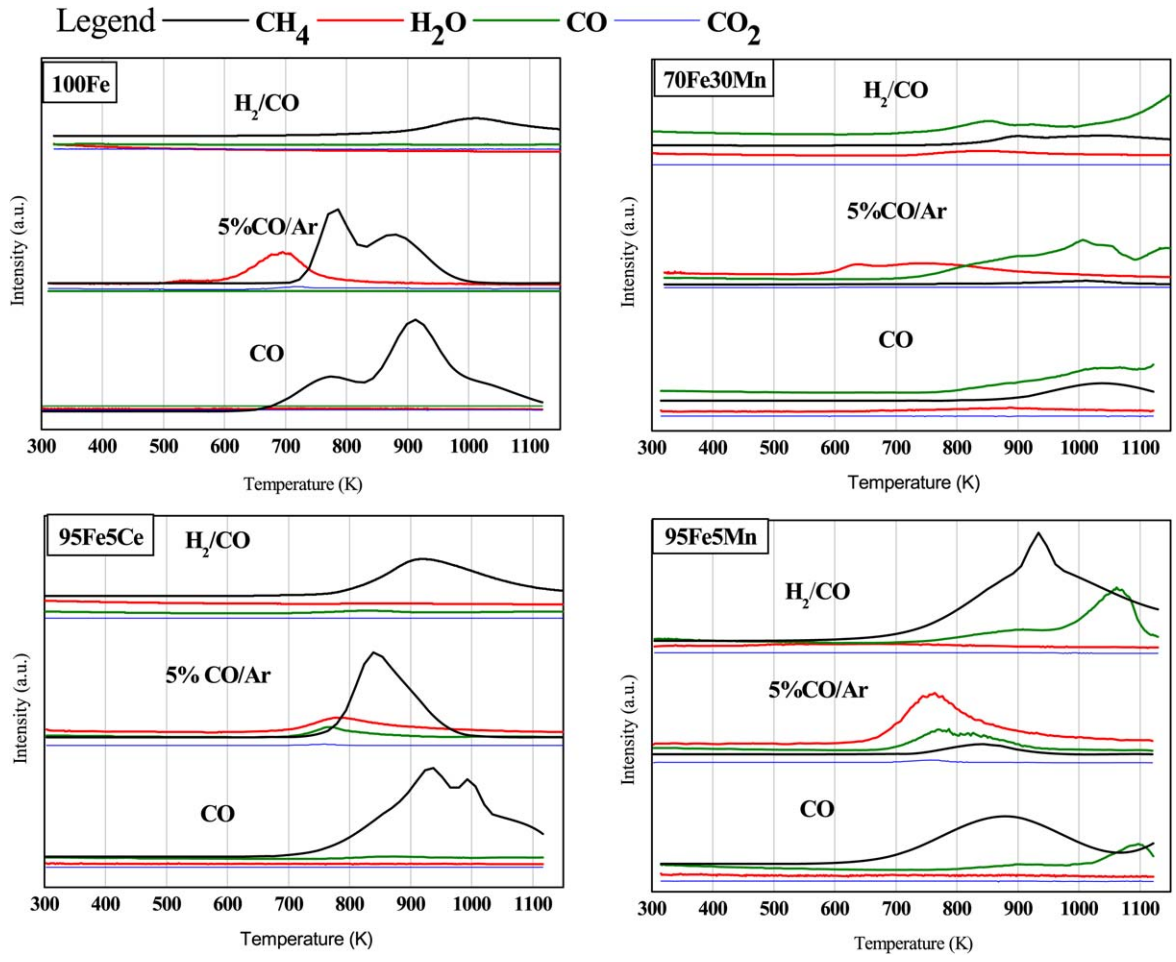

(A)

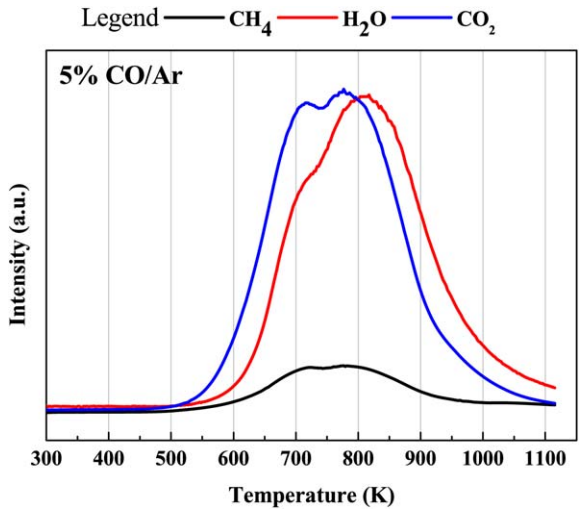

(B)

Fig. 1. (A) TPSR-H_2 of samples after activation pretreatments (5% CO/Ar, CO, or H_2/CO at 723 K for 1 h); (B) TPSR-syngas of sample 100Fe after activation treatment in 5% CO/Ar.

Fe_3O_4 and Fe–Mn mixed oxide, supporting the hypothesis that iron oxide was not fully reduced under diluted CO. In addition, two peaks at ca. 1300 and 1600 cm^{-1}, ascribed to disordered and ordered graphitic species, respectively, were observed after pure CO or H_2/CO pretreatment [32]. The relative intensity of such peaks depended on the nature of the pretreatment. The relative abundance of such species was higher when syngas was used than under carbon monoxide. It is noteworthy that a mixed iron–manganese phase was detected in both fresh and pretreated 70Fe30Mn samples. This result points to a lower carburization level of sample 70Fe30Mn compared with the rest of the series. Raman spectra of the samples pretreated under pure

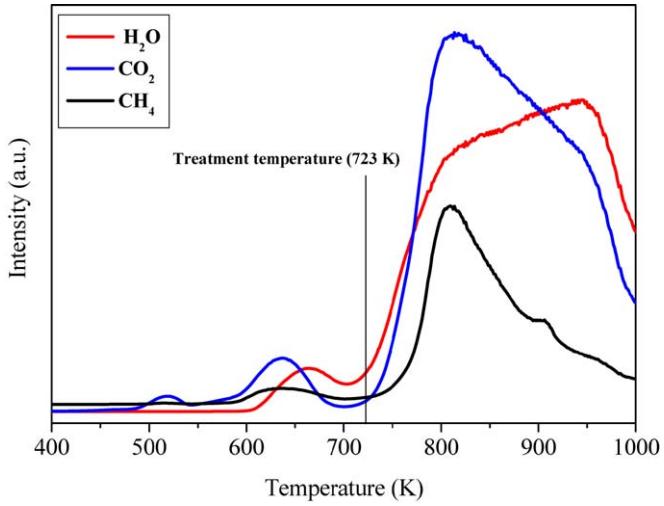

Fig. 2. Temperature-programmed reduction of sample 100Fe under $CO + H_2$.

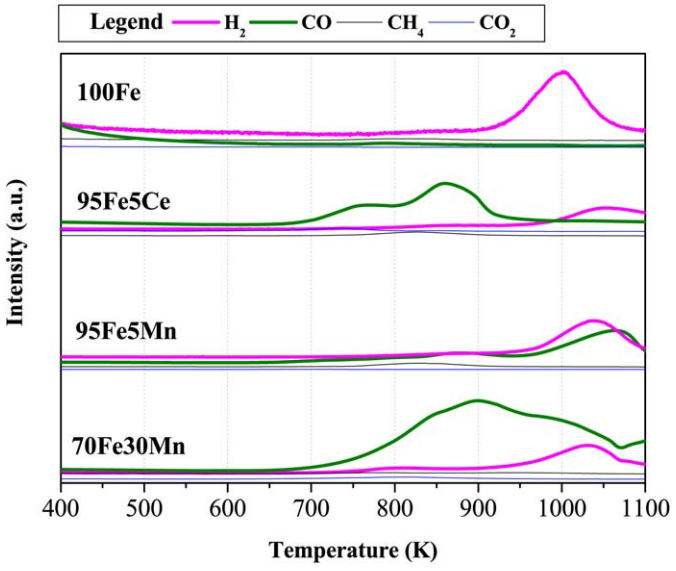

Fig. 3. TPSR-Ar of samples after H_2/CO activation pretreatments at 723 K for 1 h.

CO and syngas and subjected to TPSR-H_2, once passivated, were also recorded (data not shown). It was observed that the two graphitic bands remained relatively stable; that is, graphitic species were stable during FTS. During TPSR-H_2, methane formation was observed, but the abundance of the graphitic species was not diminished. These graphite species are not precursors of the production of hydrocarbons and do not impede their formation. In other words, they are mere spectators, at least at certain concentrations. A higher concentration of such graphitic species might block the access of the reactants to the active sites, acting thus as poisoning species rather than as mere spectators.

XRD analysis of the pretreated and subsequently passivated samples endorses the assignments of the species deduced from the other characterization techniques. The diffractograms of the samples subjected to different pretreatments are depicted in Fig. 5. A summary of the nature of the different species detected from the XRD analysis after the different pretreatments

Table 1
Phases detected by XRD after activation pretreatments and temperature programmed experiments

Sample	Pretreatment	Phases after pretreatment	Phases after TPDc-Ar	Phases after TPSR-H_2
100Fe	5% CO/Ar	Fe^0; Fe_3O_4 θ-Fe_3C	Fe^0; θ-Fe_3C	Fe^0
	CO	θ-Fe_3C		Fe^0
	H_2/CO	χ-$Fe_{2.5}C$		Fe^0; θ-Fe_3C Fe_3O_4 (traces)
95Fe5Ce	5% CO/Ar	Fe^0; Fe_3O_4 θ-Fe_3C	Fe^0; θ-Fe_3C	Fe^0
	CO	θ-Fe_3C		Fe^0
	H_2/CO	χ-$Fe_{2.5}C$		Fe^0; θ-Fe_3C Fe_3O_4 (traces)
95Fe5Mn	5% CO/Ar	Fe^0; Fe_3O_4 θ-Fe_3C	Fe^0; θ-Fe_3C	Fe^0; θ-Fe_3C
	CO	θ-Fe_3C		θ-Fe_3C
	H_2/CO	χ-$Fe_{2.5}C$	Fe^0 (traces) θ-Fe_3C	θ-Fe_3C
70Fe30Mn	5% CO/Ar	Fe^0; Fe_3O_4 FeO	Fe^0; FeO	Fe^0; θ-Fe_3C $Fe_xMn_{1-x}O$
	CO	θ-Fe_3C $Fe_xMn_{1-x}O$		θ-Fe_3C $Fe_xMn_{1-x}O$
	H_2/CO	χ-$Fe_{2.5}C$ $Fe_xMn_{1-x}O$	θ-Fe_3C $Fe_xMn_{1-x}O$	θ-Fe_3C $Fe_xMn_{1-x}O$

Note. χ-$Fe_{2.5}C$: Hägg carbide; θ-Fe_3C: cementite; Fe^0: metallic iron; Fe_3O_4: magnetite; $Fe_xMn_{1-x}O$: manganowustite.

is shown in Table 1. The assignment of the different Fe carbide phases (θ-Fe_3C and χ-$Fe_{2.5}C$) from the X-ray diffractograms should be performed carefully because they showed similar diffraction patterns. Peak assignation was based on the characteristic Bragg angles of θ-Fe_3C (JCPDS 76-1877) at 78.0° and 70.1°, which are not present in the diffractogram of the sample χ-$Fe_{2.5}C$ (JCPDS 36-1248). The relative intensity of the diffraction peaks was also taken into account for the correct identification of the carbide species.

Metallic iron (Fe^0) was the only species detected by XRD after hydrogen pretreatment. Metallic iron was also the most abundant crystalline species detected in samples 100Fe, 95Fe5Ce, and 95Fe5Mn after pretreatment with diluted CO. Fe_3O_4 and cementite (θ-Fe_3C) phases were also detected. The X-ray diffractograms of sample 70Fe30Mn displayed reflections from either wustite or manganowustite (an accurate assignment of the phases was difficult due to the low intensity of the reflections) and Fe_3O_4 phases. In contrast, diffractograms of the samples pretreated with pure CO presented only reflections ascribed to cementite (θ-Fe_3C). Sample 70Fe30Mn showed reflections ascribed to manganowustite, in agreement with the Raman analysis (Fig. 4). The diffractograms of the samples pretreated with syngas displayed reflections from the Hägg carbide (χ-$Fe_{2.5}C$). Again, sample 70Fe30Mn exhibited reflections arising from a manganowustite phase, in good agreement with the Raman analysis. All of the patterns displayed a broad reflection centered at 2θ angles of ca. 25° attributed to carbonaceous deposits. After the temperature-programmed experiments with Ar (TPD-Ar) of the samples pretreated with diluted CO,

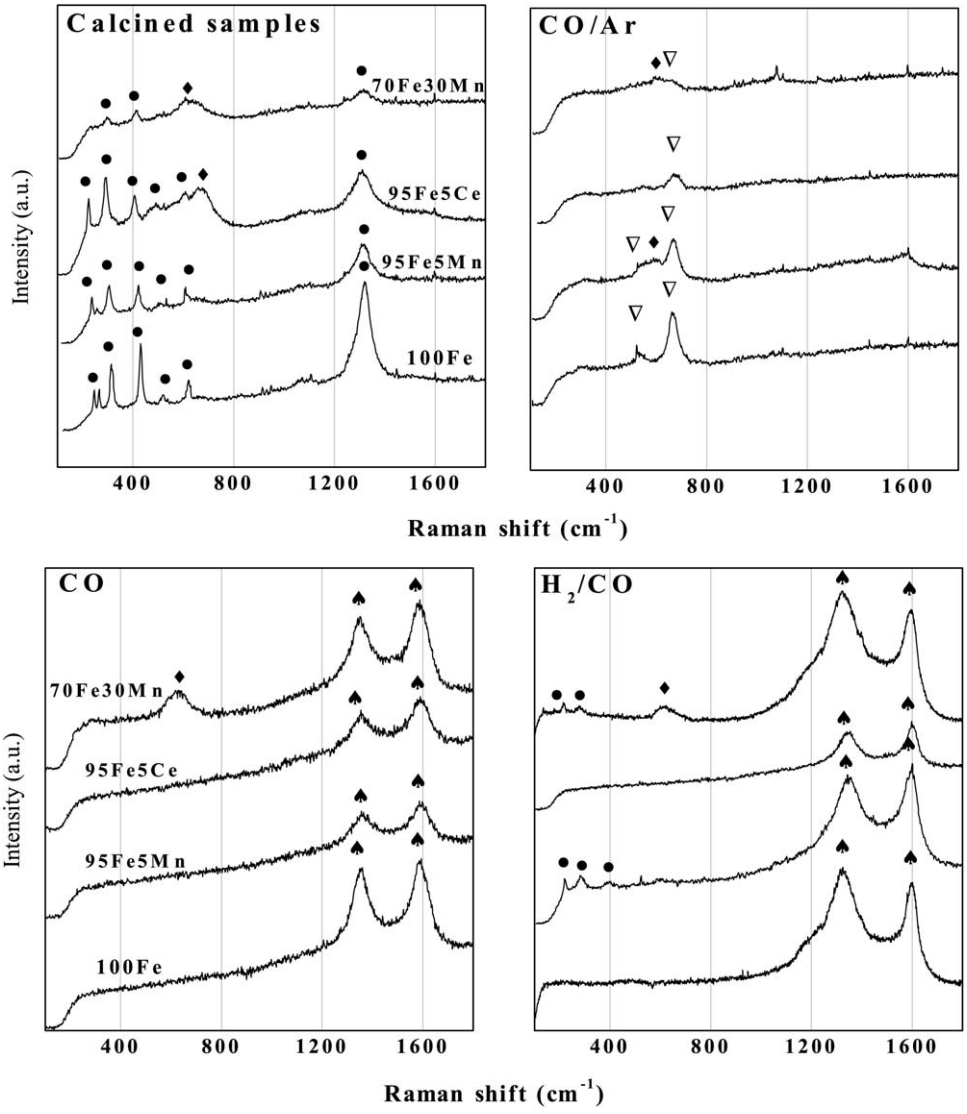

Fig. 4. Raman spectra of samples after activation pretreatments (5% CO/Ar, CO, or H_2/CO at 723 K for 1 h): (●) Fe_2O_3, (▽) Fe_3O_4, (♠) graphite, (◆) Fe–Ce or Fe–Mn mixed oxide.

metallic iron and cementite were observed. Cementite was also detected in all samples after TPSR-H_2 of the solids pretreated with both CO (pure or diluted) and H_2/CO. In the latter case, the Hägg carbide evolved to cementite, as reported by Hofer [9], with the relative abundance of cementite and metallic iron depending on the nature of the sample. In the samples pretreated with pure CO or H_2/CO, the diffraction patterns of graphite were also observed even after temperature-programmed treatments with Ar or H_2, indicating the high stability of these graphite-like species.

3.2. Catalytic performance

The samples pretreated with the different reactive atmospheres were tested in the FTS reaction at 573 K for 10,000 min. The CO conversion versus time-on-stream plots for samples 100Fe, 95Fe5Ce, and 95Fe5Mn are depicted in Fig. 6; the results for sample 70Fe30Mn are not shown, because of the low activity. As a general trend, syngas pretreatment yielded the most active catalysts in terms of CO conversion, whereas hydrogen pretreatment led to the less active materials of the series. Only moderate CO conversion differences were detected when sample 100Fe was pretreated with pure or diluted CO, the latter being slightly more efficient. The CO conversion value was independent of the oxide additive when the samples were activated with syngas. However, the differences in CO conversion between the promoted and nonpromoted samples became more evident when the activation protocol was performed in CO, following the order 95Fe5Ce > 95Fe5Mn ≈ 100Fe ≫ 70Fe30Mn.

A common and intriguing feature is that all of the samples seemed to undergo reconstruction after ca. 1000 min on stream, increasing their catalytic activity from that time on. This feature was less pronounced when the samples were activated with hydrogen, requiring more time to achieve any increase in catalytic activity. A similar behavior has been ascribed to surface reconstruction of the catalyst [10].

Table 2 collects the catalytic results of selected samples. The selectivity toward the different Fischer–Tropsch products

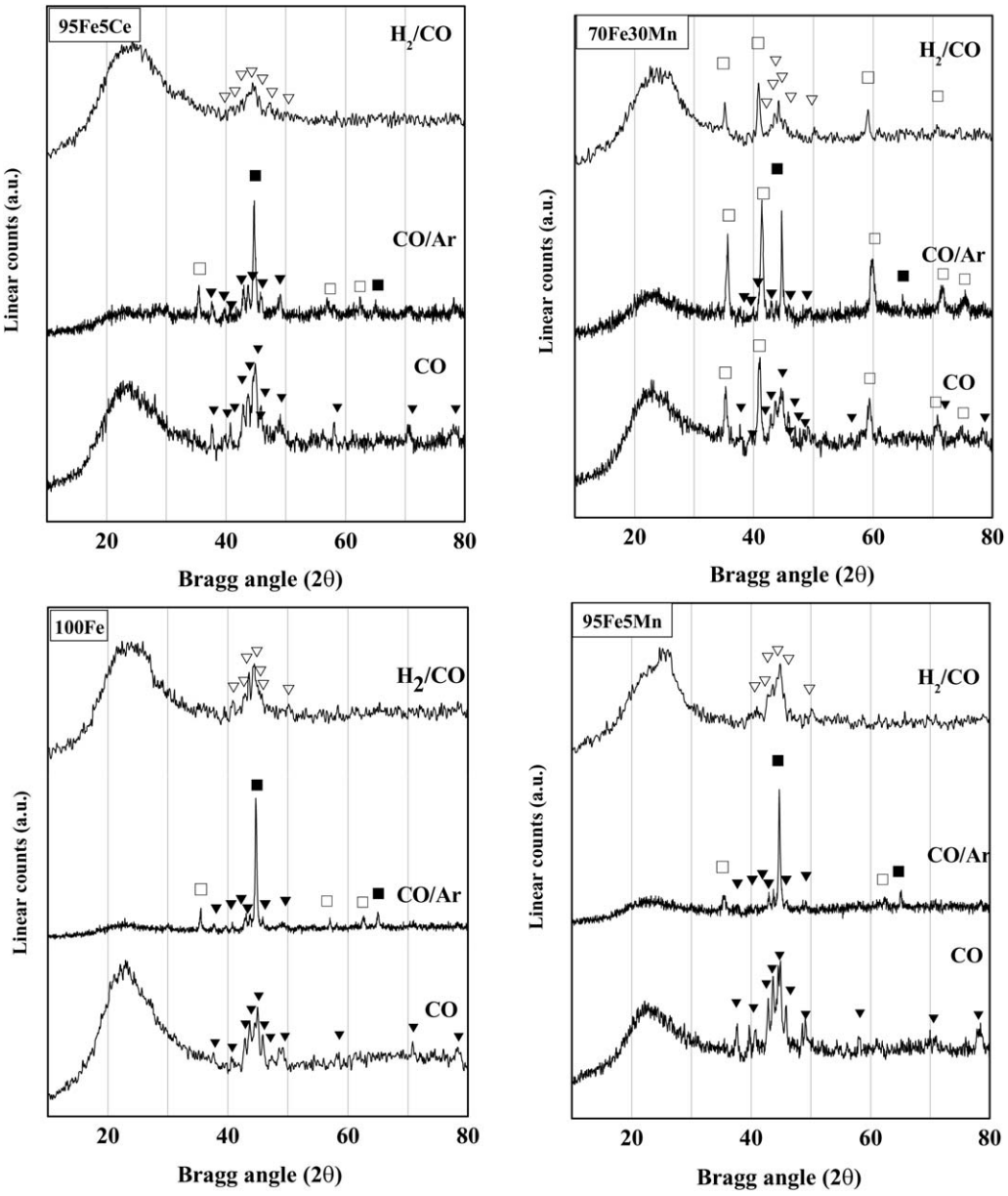

Fig. 5. Diffraction patterns of samples after activation pretreatments (5% CO/Ar, CO, or H_2/CO at 723 K for 1 h): (■) Fe^0, (□) γ-Fe_3O_4, (▼) θ-Fe_3C, (▽) χ-$Fe_{2.5}C$.

(–CH_2 units) was independent of the time on stream (data not shown). The selectivity toward carbon dioxide was higher for the Ce- and Mn-loaded samples, probably due to their higher activity in the water-gas shift reaction when activated with CO (either pure or diluted). The same applies to the hydrogen pretreatment, albeit to a lesser extent.

We must remark that product selectivity did not change with reaction time, even after reconstruction of the catalyst surface. This finding indicates that reconstruction involves the formation of more active sites, with their nature remaining unaltered. When samples were pretreated under CO, the rate of formation of active sites was increased by the oxide additive (Mn or Ce), thus reaching the steady state before. In that sense, it is worth recalling that the relationship between the surface area and the activity of the samples can be drawn only when the nature of the active sites is similar [25]. Therefore, evaluating catalyst activity by extrapolating and comparing the surface area values with different active species (cementite or the Hägg carbide) may be inaccurate.

3.3. Characterization of catalysts after reaction

After reaction, selected catalysts were studied by Mössbauer spectroscopy. The samples were passivated by following the protocol already described. Fig. 7 depicts the spectra obtained with catalyst 95Fe5Mn activated with different pretreatment gases. All of the spectra showed a complex pattern comprising magnetic and paramagnetic components. The extent of the magnetic hyperfine splitting, smaller than that of the α-Fe, was in the range typical of the iron carbides [18,33]. The shape of the magnetic component also revealed that it comprised at least three distinct sextets. The spectrum of the CO-pretreated sam-

Table 2
Activity and selectivity of selected samples after 10,000 min

Catalyst	Pretreatment[a]	X_{CO}[b]	HC[c]	O/P[d]	α[e]	CO_2[f] (%)	Product selectivity			
							CH_4	C_2–C_5	C_6–C_{12}	C_{13+}
100Fe	H_2	23	27	1.1	0.57	15.0	19.4	60.8	16.7	3.0
	CO	37	38	1.1	0.58	14.8	15.8	59.2	22.3	2.0
	H_2/CO	74	72	1.0	0.58	24.7	15.9	62.3	19.5	2.0
95Fe5Mn	H_2	27	27	1.4	0.65	24.0	14.8	46.2	35.7	2.3
	CO	48	48	1.3	0.61	24.5	14.5	49.0	34.2	1.3
	H_2/CO	64	72	1.1	0.63	26.9	11.3	44.9	35.3	7.5
95Fe5Ce	H_2	44	48	0.7	0.55	37.4	24.8	60.1	14.6	0.5
	CO	65	68	1.1	0.58	22.2	19.5	52.6	26.8	0.9
	H_2/CO	81	70	0.9	0.57	30.7	17.8	53.4	28.1	0.6

Note. Reaction conditions: 573 K, 1.01 MPa, $H_2/CO = 2$ (GHSV = 0.0023 L g^{-1} s^{-1}).
[a] Activation pretreatment.
[b] Carbon monoxide conversion (%).
[c] Hydrocarbon production expressed as $g_{CH_2}/g_{Fe}/s$ ($\times 10^5$), CH_4 free.
[d] Olefin-to-paraffin ratio.
[e] Chain growth probability.
[f] CO_2 free. Selectivity to oxygenates was negligible (<1.0%) in all cases.

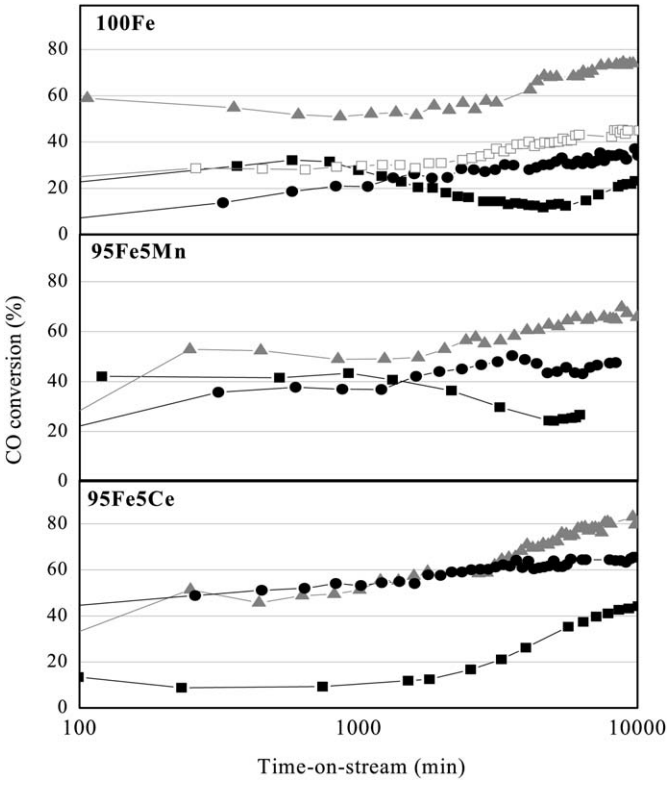

Fig. 6. Carbon monoxide conversion vs time-on-stream for samples 100Fe, 95Fe5Mn, and 95Fe5Ce after activation pretreatments (33% H_2/N_2, 16 h/673 K, 5% CO/Ar, CO, or H_2/CO at 1 h for 723 K). (■) H_2, (▲) H_2/CO, (●) CO, (□) CO/Ar.

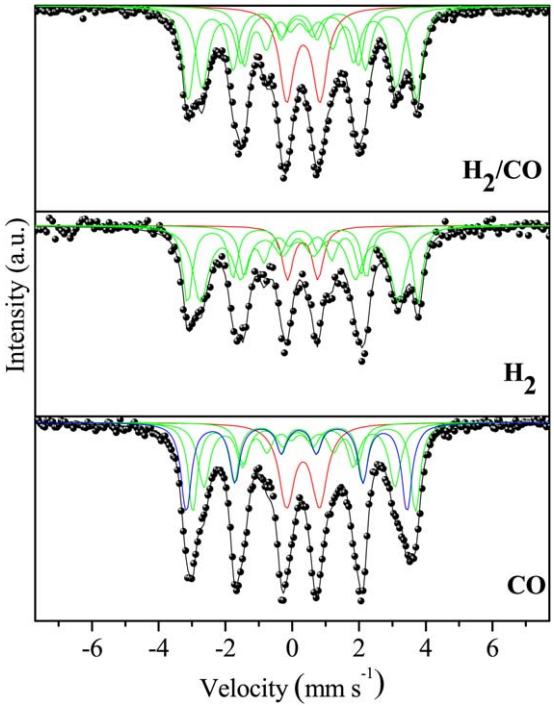

Fig. 7. Mössbauer spectra of sample 95Fe5Mn activated in H_2, CO, and H_2/CO after catalytic reaction for ca. 10,000 min. The computer fittings are shown as solid lines.

ple appeared to be different from the other two spectra, which were both very similar. It is known that the Mössbauer spectrum of some iron carbides is formed by various sextets, and that determining the number of the constituent sextets and their relative intensities, as well as their corresponding hyperfine magnetic fields, is essential to reliably identifying the different carbide phases. Thus, the spectra were fitted to three sextets (1, 2, and 3) and a doublet. Moreover, a fourth sextet had to be included for the CO-pretreated sample to accomplish a consistent fitting of the spectrum. We attempted to improve the fitting of the H_2-pretreated sample by introducing an additional Fe^{2+} doublet, but the relative spectral area obtained for this doublet was too small (≅1%), and the fitting result did not improve significantly with respect to that obtained by fitting only one doublet and the three sextets. The fitted spectra are shown in Fig. 7, and the Mössbauer parameters obtained from the fittings are collected in Table 3. The obtained parameters allowed

Table 3
Mössbauer parameters of sample 95Fe5Mn after reaction for 10,000 min (activated with H_2, CO and H_2/CO)

		H_2	H_2/CO	CO
Doublet (superparamagnetic Fe^{3+})	δ_D (mm s^{-1})	0.31 (2)	0.33 (1)	0.32 (1)
	Δ_D (mm s^{-1})	0.91 (5)	0.99 (2)	0.98 (2)
	Γ_D (mm s^{-1})	0.40 (4)	0.52 (2)	0.56 (4)
	A_D (%)	11.0	19.8	17.4
Sextet 1 (χ-$Fe_{2.5}C$)	δ_{S1} (mm s^{-1})	0.20 (3)	0.19 (1)	0.19 (2)
	$2\varepsilon_{S1}$ (mm s^{-1})	0.02 (2)	0.02 (1)	0.02 (2)
	H_{S1} (T)	18.4 (2)	18.0 (1)	17.7 (1)
	Γ_{S1} (mm s^{-1})	0.54 (3)	0.44 (3)	0.44 (4)
	A_{S1} (%)	43.0	30.0	21.3
Sextet 2 (χ-$Fe_{2.5}C$)	δ_{S2} (mm s^{-1})	0.24 (3)	0.25 (1)	0.24 (2)
	$2\varepsilon_{S2}$ (mm s^{-1})	0.07 (3)	0.03 (1)	0.00 (2)
	H_{S2} (T)	10.8 (1)	10.6 (1)	10.6 (1)
	Γ_{S2} (mm s^{-1})	0.36 (4)	0.40 (3)	0.40 (2)
	A_{S2} (%)	18.5	18.7	12.5
Sextet 3 (χ-$Fe_{2.5}C$)	δ_{S3} (mm s^{-1})	0.27 (1)	0.26 (1)	0.28 (3)
	$2\varepsilon_{S3}$ (mm s^{-1})	0.05 (1)	0.05 (1)	0.08 (3)
	H_{S3} (T)	21.4 (1)	21.2 (1)	20.7 (1)
	Γ_{S3} (mm s^{-1})	0.34 (3)	0.40 (2)	0.34 (2)
	A_{S3} (%)	27.6	31.5	23.3
Sextet 4 (θ-Fe_3C)	δ_{S4} (mm s^{-1})			0.17 (3)
	$2\varepsilon_{S4}$ (mm s^{-1})			0.03 (3)
	H_{S4} (T)			20.5 (1)
	Γ_{S4} (mm s^{-1})			0.38 (4)
	A_{S4} (%)			25.4
χ^2		1.2	2.8	1.7

Note. δ = isomer shift (relative to α-Fe); Δ = quadrupole splitting; 2ε = quadrupole shift; Γ = full line width at half maximum; H = magnetic hyperfine field; A = relative spectral area; χ^2 = normalized chi-squared. Numbers in brackets indicate the error in the last figure.

assignment of the three sextets labeled 1, 2, and 3 to Hägg carbide (χ-$Fe_{2.5}C$) and sextet 4 to cementite (θ-Fe_3C) [18,34]. Superparamagnetic or amorphous ferric oxides and even substituted iron oxides [35] produced parameters similar to those obtained for doublet D. This finding precluded an unequivocal assignment of this doublet. A quadrupole doublet analogous to this one was the dominant component in the spectrum of a Fe_2O_3/K_2O/SiO_2/CuO catalyst after the Fischer–Tropsch reaction, due to a mixture of superparamagnetic particles of both magnetite and hematite phases [35]. In summary, Mössbauer data showed that samples pretreated with hydrogen or syngas after reaction contained similar species, Hägg carbide and probably superparamagnetic ferric oxides, whereas an additional carbide phase, cementite, was present in the CO-activated sample.

4. Discussion

4.1. Identification of the phases formed after the pretreatment

Scheme 2 depicts the routes of formation and the most stable species obtained during the different pretreatments. Scheme 3 summarizes the different samples, activation pretreatments, temperature-programmed experiments, desorbed species, and phases detected.

Bartholomew et al. [20,21] have identified up to six different carbonaceous species onto the surface of iron-based catalysts after the FTS reaction. The reactivity of these species was assigned from the temperature value of the methane formation peak in the TPSR-H_2; that is, the more reactive the species, the lower formation temperature. The identified species (in order of reactivity) were $C_\alpha > C_\beta > C_\gamma > C_\delta$. Two different C_γ and C_δ species were reported. C_α is atomic carbonaceous species resulting from the dissociative adsorption of CO; C_β is a polymeric (2–3 atoms) surface carbonaceous species. C_γ is iron carbide, either ε'-$Fe_{2.2}C$ or χ-$Fe_{2.5}C$. Finally, C_δ are graphite-type carbonaceous species that are both ordered and less ordered, as described above. The first peak of methane formation is due to the presence of C_α-type species that, according to our results, appear at 770 K in sample 100Fe when pretreated in CO (Fig. 1). In contrast, they were not observed in the promoted samples or after syngas pretreatment, probably due to the fact that under syngas, C_α species are prone to react with H_2, forming methane, as explained above. The appearance of a methane formation peak at 870–900 K (after treatment with CO) or at 920–950 K (after treatment with syngas) was ascribed to the presence of C_β-type species. Methane formation at 1000 K was observed. This process was assigned to the hydrogenation of iron carbides (θ-Fe_3C and χ-$Fe_{2.5}C$), which were also identified by XRD. The former, cementite, is the most evolved iron carbide species [9] and was detected only after pretreatment with CO. The latter, the Hägg carbide, was stabilized after the pretreatment with syngas. Other iron carbide species, such as ε'-$Fe_{2.2}C$, were not detected. This type of carbide has been only detected in silica-supported iron catalysts and in massive iron samples treated with syngas at low temperatures (513 K) [18].

Cementite is transformed into methane and metallic iron at 1000 K with hydrogen, as was revealed by the XRD analysis of CO pretreated 100Fe and 95Fe5Ce samples subjected to TPSR-H_2 experiments. However, methane formation was not observed for the Mn-containing samples. Furthermore, cementite phases were still observed by XRD analysis of these samples after TPSR-H_2. It seemed that the presence of Mn impeded cementite decomposition, probably by decreasing H_2 chemisorption.

The Hägg carbide (χ-$Fe_{2.5}C$) is decomposed into methane and cementite at ca. 1050 K with hydrogen. This finding was confirmed by the X-ray diffractograms of the samples pretreated with syngas and subjected to TPSR-H_2.

The graphite-type species were observed in both the XRD patterns and the Raman spectra of the samples pretreated with H_2/CO and CO. As discussed above, such species are stable under hydrogen (TPSR-H_2) and oxygen below 650 K (data not shown). When thermal analysis of the species formed after the different pretreatment was conducted under Ar, hydrogen was desorbed.

Syngas pretreatment led to formation of χ-$Fe_{2.5}C$. As deduced from the TPSR-H_2 experiments, this phase is prone to stabilize C_β-type species. However, cementite was the only iron carbide detected after CO pretreatment. Sample 100Fe showed

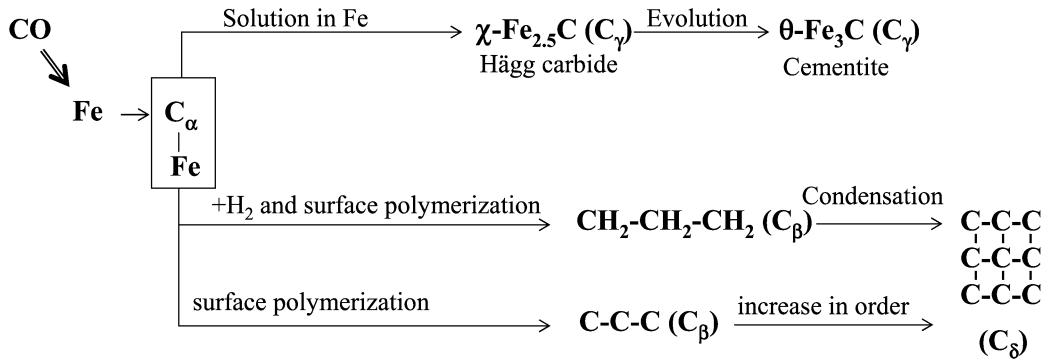

Scheme 2. Routes of formation of the carbonaceous species after pretreatments in CO and H_2/CO (adapted from Ref. [21]).

both C_α and C_β species after pretreatment with CO. The promoted samples (95Fe5Ce and 95Fe5Mn) displayed more C_β species than sample 100Fe. Sample 70Fe30Mn behaved differently; carbide formation was low, and mixed Fe–Mn oxide phases (manganowustite) were clearly detected.

4.2. Structure–reactivity relationship

As stated above, syngas pretreatment yielded the most active catalysts irrespective of the sample composition. This result agrees well with the finding that the nature of the surface species after syngas activation was similar for all samples, with all samples displaying a methane formation peak ascribed to C_β. Hematite (α-Fe_2O_3) evolved into the Hägg carbide (χ-$Fe_{2.5}C$) that, in the presence of hydrogen, cannot develop into cementite (θ-Fe_3C).

The chemical composition of the sample played a key role on its catalytic performance only if activated under CO. Cementite (θ-Fe_3C) was detected in all samples pretreated in pure CO, with C_α species stabilized on the surface, as revealed by the TPSR-H_2 experiments. In promoted samples (95Fe5Ce and 95Fe5Mn), methane formation peaks arising from C_β species displayed higher areas than those arising from the C_β species stabilized over the nonpromoted samples; that is, there were more C_β species over promoted samples. Interestingly, the Mn- and Ce-loaded samples, even when displaying fewer C_α species, developed more active catalysts than sample 100Fe, revealing that C_β is more closely related to FTS activity than C_α.

Finally, when the samples were pretreated with CO/Ar, magnetite (Fe_3O_4) and metallic iron were also detected. However, the resulting catalysts displayed higher activity than when the samples were treated under pure CO.

Bartholomew et al. [20,21] established a straightforward relationship between the amount of surface active species (quantified from the methane formation peaks detected in the TPSR-H_2 experiments) and FTS activity. However, methane is not a representative Fischer–Tropsch product because it is not formed from the polymerization of the monomeric $–CH_2–$ units [36]. That is, whereas methane can be produced during FTS by the hydrogenation of C_α species, a proper Fischer–Tropsch product results from the hydrogenation of already polymerized $(–CH_x–)_n$ species (i.e., C_β), yielding hydrocarbons. However, C_β would yield methane rather than polymerized species at atmospheric pressure only at a higher temperature than that for C_α. This line of argument justifies our findings. The samples activated with CO, although having more C_α species, were less active in FTS. On the other hand, the samples activated with syngas, displaying a larger amount of C_β, were more active in FTS. Equally important, an unequivocal correlation between the nature of the iron carbide phase and the predominant surface carbonaceous species can be drawn from this study. The activation with CO rendered the most evolved iron carbide phase, i.e., cementite, over which C_α species were stabilized, as it is inferred from the TPSR-H_2 experiments and confirmed by XRD results. On the contrary, χ-$Fe_{2.5}C$ was formed with syngas, promoting the stabilization of surface C_β species. The higher activity was achieved when the samples were activated with syngas. Therefore, the presence of surface C_β species could be related with the activity in FTS. This explains why the sample 100Fe was more active when it was activated with diluted CO than with pure CO, in spite of the larger amount of carbide species observed after the latter pretreatment. As discussed above, cementite, metallic iron and magnetite were formed after CO/Ar pretreatment. Once the activated sample entered in contact with syngas (during FTS), the noncarburized iron species (metallic iron and magnetite) developed the Hägg carbide, resulting in a more active catalyst than seen in pure CO treatment. This result agrees well with the findings of Schulz et al. [16] in the sense that such a carbide phase is the most active in FTS.

Further evidence supporting the finding that the amount of methane formed in the TPSR-H_2 experiments cannot be straightforwardly related to FTS activity is depicted in Fig. 8. This figure shows the TPSR-H_2 profiles of sample 100Fe activated with syngas at 553 and 723 K. Activation produced a more active catalyst for FTS at 723 K ($X_{CO} = 60\%$) than at 553 K ($X_{CO} = 35\%$). However, methane desorption after pretreatment at 553 K was centered at ca. 770 K, being shifted up to 1000 K for the sample pretreated at 773 K. As stated above, methane desorption at ca. 1000 K is ascribed to the C_β species, whereas C_α renders methane at lower temperatures. In the case of high-temperature pretreatment, methane formation from the C_α species occurred during the pretreatment and thus was not detected.

The effect of the nature of the pretreatment gas on the catalytic performance of the different samples was clear for sam-

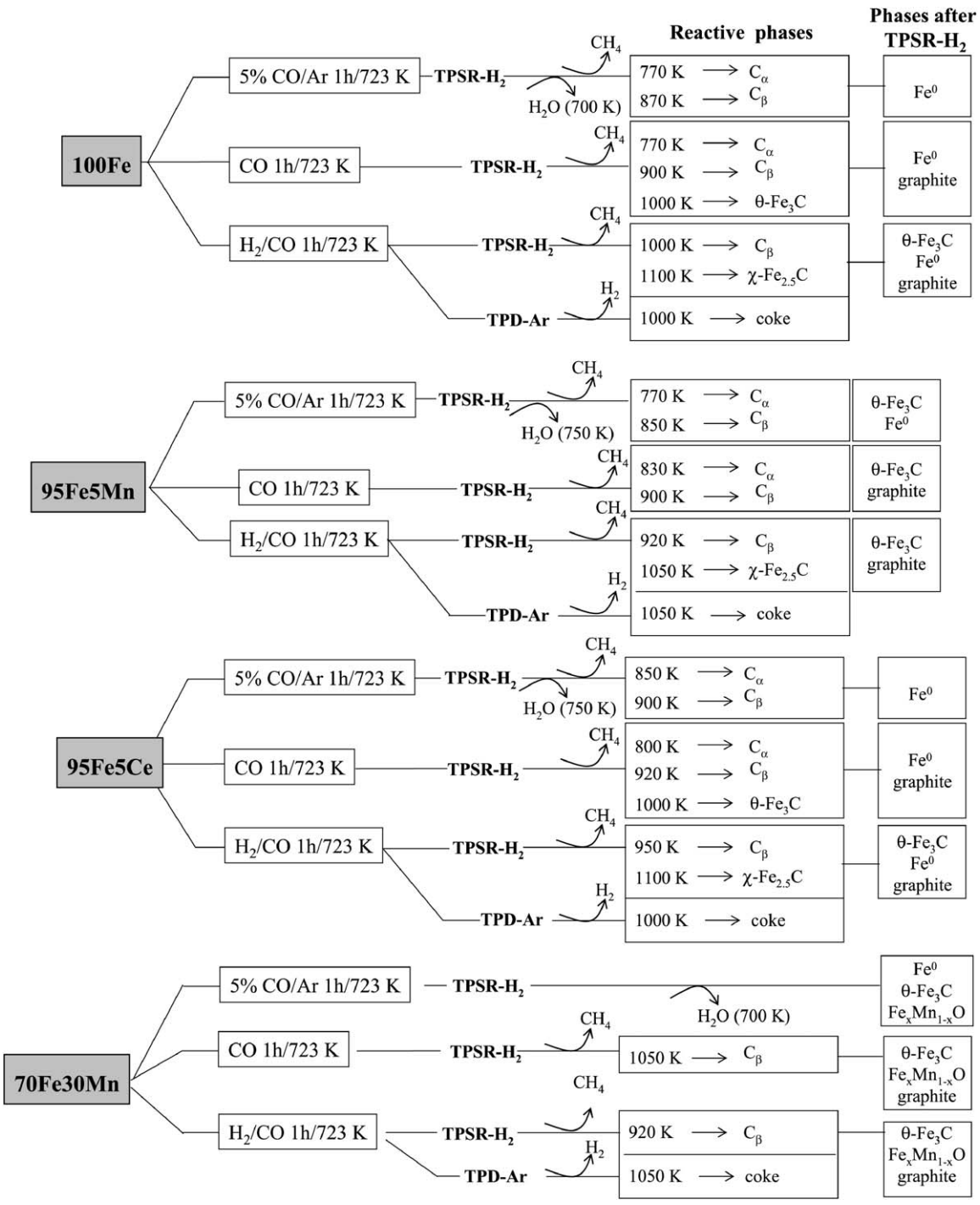

Scheme 3. Activation pretreatments, temperature programmed experiments, desorbed species and phases detected for the different samples.

ple 100Fe. However, the differences in the catalytic behavior were less obvious for the Ce- and Mn-containing samples, because those metals are known to increase carbon monoxide chemisorption and to prevent C_α hydrogenation in some extent, thereby stabilizing the C_β species.

We have proposed that the C_β species are the intermediates in FTS and that the Hägg carbide (χ-$Fe_{2.5}C$) is the active species. The FTS activity of the samples pretreated with CO was lower because cementite (θ-Fe_3C) was the species formed. However, such samples displayed an increasing activity with time in FTS, displaying higher CO conversion levels at the steady state (10,000 min), although lower than those corresponding to the samples pretreated with syngas. The Mössbauer spectroscopy results show that cementite can evolve into the Hägg carbide under FTS reaction conditions, thus yielding catalysts as active as in the case of pretreatment with syngas. However, the extent of this transformation is limited, as evidenced by the detection of cementite phases in the used catalyst. Consequently, fewer active sites for FTS are found in the samples pretreated with CO than in those pretreated with syngas.

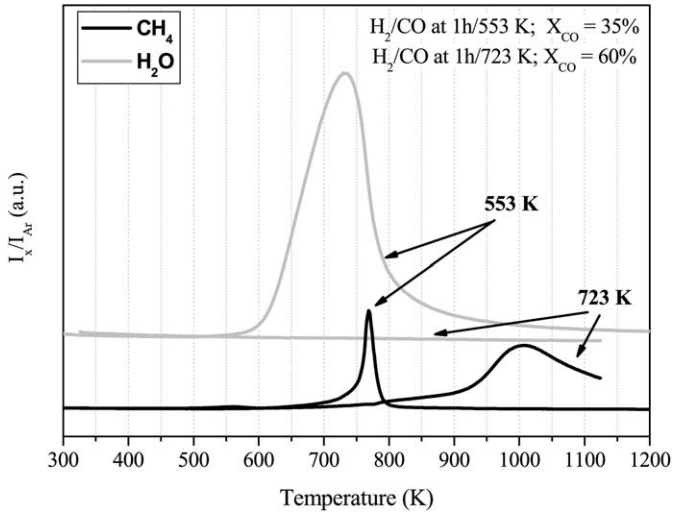

Fig. 8. TPSR-H_2 profiles of sample 100Fe activated under syngas at 553 and 723 K.

5. Conclusion

When iron oxide (hematite) was pretreated with H_2, CO, and H_2/CO, this material was transformed into different catalysts. Only metallic iron was formed when the pretreatment was carried out with hydrogen. However, iron carbide, mainly cementite, was formed with CO (pure or diluted) pretreatments. In contrast, the Hägg carbide, rather than the most evolved cementite carbide, was formed when the pretreatment was performed with syngas. Surface carbonaceous species were stabilized on both types of iron carbides. C_α species were stabilized on cementite (θ-Fe_3C), whereas C_β species were stabilized on the Hägg carbide (χ-$Fe_{2.5}C$). θ-Fe_3C species were less active in FTS, although they can evolve in the reaction medium into the more active species, the Hägg carbide, over which C_β intermediates are formed. The extent of this transformation is not complete, and therefore, some cementite species remain stable. Mn and Ce promotion is effective only when the samples are activated with CO, thus favoring the stabilization of C_β species even on cementite.

Acknowledgments

S. Rojas acknowledges the "Programa Ramón y Cajal" of MEC, Spain, for financial support. F.J. Pérez-Alonso also thanks MEC, Spain for a predoctoral fellowship. Financial support from MEC, Spain (ENE2004-07345-c03-01/A) and from the EU (ENKT6-CT-2002-00682) is acknowledged. The authors thank Dr. M. Gracia (Instituto de Química Física "Rocasolano," CSIC) for the Mössbauer study and Dr. M.L. Granados (ICP-CSIC) for valuable comments.

References

[1] R.B. Anderson, in: P.H. Emmett (Ed.), Catalysis, Van Nostrand–Reinhold, New York, 1956, p. 29.
[2] R.J. O'Brien, L. Xu, R.L. Spicer, B.H. Davis, Energy Fuels 10 (1996) 921.
[3] D.B. Bukur, M. Koranne, X. Lang, K.R.P.M. Rao, J.S. Hwang, Appl. Catal. A Gen. 126 (1995) 85.
[4] M.E. Dry, in: J.R. Anderson, M. Boudart (Eds.), Catalysis—Science and Technology, Springer-Verlag, New York, 1981, p. 59.
[5] H. Kölbel, M. Ralek, Catal. Rev. Sci. Eng. 21 (1980) 225.
[6] D.B. Bukur, X.S. Lang, Y.J. Ding, Appl. Catal. A Gen. 186 (1999) 255.
[7] J.C.W. Kuo, Slurry Fischer–Tropsch/Mobil Two-Stage Process of Converting Syngas to High Octane Gasoline, DOE/PC/30022-10, Final Report, June 1983.
[8] J.C.W. Kuo, Slurry Fischer–Tropsch/Mobil Two-Stage Process of Converting Syngas to High Quality Transportation Fuels, DOE/PC/60019-9, Final Report, 1985.
[9] P.H. Emmett (Ed.), Crystallite Phase and Their Relationship to Fischer–Tropsch Catalysis, Reinhold, New York, 1956, p. 407.
[10] H. Schulz, G. Schaub, M. Claeys, T. Riedel, Appl. Catal. A Gen. 186 (1999) 215.
[11] M.D. Shroff, D.S. Kalakkad, K.E. Coulter, S. Kohler, M.S. Harrington, N.B. Jackson, A.G. Sault, K.D. Abhaya, J. Catal. 156 (1995) 185.
[12] F. Blanchard, J.P. Reymond, B. Pommier, S.J. Teichner, J. Mol. Catal. 17 (1982) 171.
[13] R.A. Dictor, A.T. Bell, J. Catal. 97 (1986) 121.
[14] C.S. Kuivila, P.C. Stair, J.B. Butt, J. Catal. 118 (1989) 299.
[15] J.A. Amelse, J.B. Butt, L.H. Scwartz, J. Phys. Chem. 82 (1978) 558.
[16] T. Riedel, H. Schulz, G. Schaub, K.W. Jun, J.S. Hwang, K.W. Lee, Top. Catal. 26 (2003) 41.
[17] G.B. Raupp, W.N. Delgass, J. Catal. 58 (1979) 361.
[18] J.W. Niemantsverdriet, A.M. van der Kraan, W.L. van Dijk, H.S. van der Baan, J. Phys. Chem. 84 (1980) 3363.
[19] R.J. O'Brien, L. Xu, D.R. Milburn, Y.X. Li, K.J. Klabunde, B.H. Davis, Top. Catal. 2 (1995) 71.
[20] S.A. Eliason, C.H. Bartholomew, Stud. Surf. Sci. Catal. 111 (1997) 517.
[21] J. Xu, C.H. Bartholomew, J. Phys. Chem. B 109 (2005) 2392.
[22] G.J. Hutchings, J.C.A. Boeyens, J. Catal. 100 (1986) 507.
[23] F.J. Pérez-Alonso, M. López Granados, M. Ojeda, P. Terreros, S. Rojas, T. Herranz, J.L.G. Fierro, M. Gracia, R. Gancedo, Chem. Mater. 17 (2005) 2329.
[24] S. Li, A. Li, S. Krishnamoorthy, E. Iglesia, Catal. Lett. 77 (2001) 197.
[25] S. Li, G.D. Meizner, E. Iglesia, J. Phys. Chem. B 105 (2001) 5743.
[26] K.B. Jensen, F.E.J. Massoth, J. Catal. 92 (1985) 109.
[27] H. Papp, F. Wieczorek, Thermochim. Acta 103 (1986) 187.
[28] T. Herranz, S. Rojas, M. Ojeda, F.J. Pérez-Alonso, P. Terreros, K. Pirota, J.L.G. Fierro, Chem. Mater. 18 (2006) 2364.
[29] T. Herranz, S. Rojas, F.J. Pérez-Alonso, M. Ojeda, P. Terreros, J.L.G. Fierro, Appl. Catal. A Gen. (2006), in press.
[30] M.D. Shroff, A.K. Datye, Catal. Lett. 37 (1996) 101.
[31] D.L.A. Faria, S.V. Silva, M.T. Oliveira, J. Raman Spectrosc. 28 (1997) 873.
[32] S.M.K. Airaksinen, M.A. Banares, A.O.I. Krause, J. Catal. 230 (2005) 507.
[33] G. Le Caer, J.M. Dubois, J.P. Senateur, J. Solid State Chem. 19 (1976) 19.
[34] E. Murad, J.H. Johnston, in: G.J. Long (Ed.), Iron Oxide and Hydroxides in Mössbauer Spectroscopy Applied to Inorganic Chemistry, Plenum, New York, 1987, p. 507.
[35] D. Mahajan, P. Gütlich, J. Ensling, K. Pandya, U. Stumm, P. Vijayaraghavan, Energy Fuels 17 (2003) 1210.
[36] M.E. Dry, J. Chem. Technol. Biotechnol. 77 (2001) 43.